Natural Resources Canada | Ressources naturelles Canada

GEOLOGICAL SURVEY OF CANADA
OPEN FILE 9172

Arsenopyrite Re-Os age and zircon U-Pb geochronology of gold prospects, Caniapiscau-Koksoak area, northern Labrador Trough, Quebec

S.T. Hébert, P. Mercier-Langevin, R.A. Creaser,
N. Wodicka, and P.-S. Ross

2024

Canada

GEOLOGICAL SURVEY OF CANADA
OPEN FILE 9172

Arsenopyrite Re-Os and zircon U-Pb geochronology of gold prospects, Caniapiscau-Koksoak area, northern Labrador Trough, Quebec

S.T. Hébert[1], P. Mercier-Langevin[2,3], R.A. Creaser[4], N. Wodicka[5], and P.-S. Ross[1]

[1]Institut national de la Recherche scientifique, Centre Eau, Terre, Environnement, 490, rue de la Couronne, Québec, Quebec

[2]Geological Survey of Canada, 490, rue de la Couronne, Québec, Quebec

[3]Present address: Agnico Eagle Mines Limited, 145 King Street East, Toronto, Ontario

[4]Earth and Atmospheric Sciences, University of Alberta, 11223 Saskatchewan Drive N.W., Edmonton, Alberta

[5]Geological Survey of Canada, 601 Booth Street, Ottawa, Ontario

2024

Permanent link: https://doi.org/10.4095/pmt3329

This publication is available for free download through the NRCan Open Science and Technology Repository (https://ostrnrcan-dostrncan.canada.ca/).

Recommended citation
Hébert, S.T., Mercier-Langevin, P., Creaser, R.A., Wodicka, N., and Ross, P.-S., 2024. Arsenopyrite Re-Os and zircon U-Pb geochronology of gold prospects, Caniapiscau-Koksoak area, northern Labrador Trough, Quebec; Geological Survey of Canada, Open File 9172, 1 .zip file. https://doi.org/10.4095/pmt3329

Publications in this series have not been edited; they are released as submitted by the author.

ISSN 2816-7155
ISBN 978-0-660-71350-2
Catalogue No. M183-2/9172E-PDF

Arsenopyrite Re-Os and zircon U-Pb geochronology of gold prospects, Caniapiscau-Koksoak area, northern Labrador Trough, Quebec

Simon T. Hébert[1], Patrick Mercier-Langevin[2,3*], Robert A. Creaser[4], Natasha Wodicka[5], and Pierre-Simon Ross[1]

[1]Institut national de la Recherche scientifique, Centre Eau, Terre, Environnement, 490, rue de la Couronne, Québec, Quebec G1K 9A9

[2]Geological Survey of Canada, 490, rue de la Couronne, Québec, Quebec G1K 9A9

[3]Present address: Agnico Eagle Mines Limited, 145 King Street East, Toronto, Ontario M5C 2Y7

[4]Earth and Atmospheric Sciences, University of Alberta, 11223 Saskatchewan Drive N.W., Edmonton, Alberta T6G 2R3

[5]Geological Survey of Canada, 601 Booth Street, Ottawa, Ontario K1A 0E8

*Corresponding author email: p.mercier-langevin@agnicoeagle.com

ABSTRACT

The Labrador Trough of northern Quebec is perhaps best known for its giant iron ore deposits, but shows exploration potential for several other deposits types, including orogenic-style gold. In the Caniapiscau-Koksoak area, gold showings are commonly associated with late structural features in mafic to intermediate intrusive rocks and their vicinity, but the timing of mineralization is unclear. In this study, we provide geochronology results on two samples. A gold-bearing arsenopyrite mineral separate from a vein in the Golden Tooth structure (Willbob property) was dated by Re-Os using negative thermal ionization mass spectrometry (N-TIMS). A weighted average model age of 1810.7 ± 4.6 Ma was obtained, representing the first direct dating of gold mineralization in the Labrador Trough. It is interpreted as the age of structurally controlled, Montagnais sill-hosted vein-style gold mineralization in the northern part of the Trough and fits within the known age of the Trans-Hudson orogeny. At the Golden Tooth showing, the mineralized veins are interpreted to have formed during the last deformation episode in the region, D_4. To provide additional geological context for the area a conglomerate from the Baby Formation (Koksoak Group) sampled on the Kan property was dated by U-Pb on zircons using a sensitive high-resolution ion microprobe (SHRIMP) and gives an estimate of the maximum age of deposition for the conglomerate at 2619 ± 11 Ma. This contrasts with regional geologic knowledge and clasts composition, which suggests that the Baby Formation is Paleoproterozoic in age rather than Archean.

INTRODUCTION

The Labrador Trough, which straddles the border between Quebec and the province of Newfoundland and Labrador, is a complex geological belt of Paleoproterozoic age. It is part of the New Quebec Orogen, which itself forms the eastern part of the Trans-Hudson Orogen that surrounds the Superior Province (Hoffman, 1988) (Fig. 1).

The Paleoproterozoic Trans-Hudson Orogen is known for its significant mineral resources, including iron deposits, volcanogenic massive sulphide (VMS) copper, zinc, lead, gold, and silver deposits, komatiite-associated nickel-copper-cobalt-platinum group element (PGEorthomagmatic deposits, and gold deposits; it is also known to have potential for other deposit types such as stratiform copper and IOCG (iron oxides, copper, gold) type systems (Gross, 1993; Corrigan et al., 2007; Corriveau et al., 2007; Galley et al., 2007; Layton-Matthews et al., 2007; Lesher, 2007). In the Labrador Trough, documented exploration activity began around 1860 and has continued intermittently until the present (Clark and Wares, 2004), with significant iron production occurring in recent decades. Several mineralized occurrences of precious metals (e.g., Au and Ag), base metals (e.g., Pb, Zn, Cu and Ni) and strategic metals (e.g., PGEs, U and rare earth elements (REE)) have also been discovered and are still the focus of considerable exploration work.

O3 Mining Inc's Kan project (a property now owned by Les Ressources Tectonic) and Midland Exploration's Willbob project, in the Caniapiscau-Koksoak sector within the northern part of the Labrador Trough, both contain several gold showings hosted in volcano-sedimentary and intermediate to mafic intrusive rocks of Proterozoic age (Trépanier and Dessureault, 2000; Lafrance et al., 2012; Richard, 2019). The characteristics of the gold mineralization, of the associated hydrothermal alteration, and of the structural controls in these sectors vary depending on the nature of the host rocks and their location in the host sequence (Hébert and Lee, 2018). The gold showings are commonly associated with well-defined structural features, suggesting a genetic relationship with regional deformation. However, several deformation events have occurred, and the role that these events played in the formation, location, subsequent modifications, and preservation of gold occurrences remains poorly understood. At the Kan property, gold mineralization is hosted in subvertical quartz veins with a predominantly E-NE and W-NW orientation (Hébert and Lee, 2018). These quartz veins seem to be contained in a system of conjugate fractures associated with a late-stage brittle deformation event. In contrast, the gold mineralizations on the Willbob property are hosted in shear zones, which appear to be late relative to the regional folding. The Kan and Willbob projects could therefore feature contemporary mineralization controlled by several distinct structural elements that are nonetheless part of the same tectonic event or the same regional deformation phase (Hébert and Lee, 2018).

The uncertainty related to the relative chronology of the mineralizing events and their association with tectonic episodes limits the scope and predictive capacity of exploration models. The results presented herein, including the first direct dating of gold mineralization in the Labrador Trough (Re-Os dating of gold-bearing arsenopyrite), along with U-Pb zircon dating of a conglomerate from the host sequence, are used to help unravel the sequence of events controlling the nature and distribution of the gold mineralization in the Caniapiscau-Koksoak sector, and to establish regional chronological correlations.

REGIONAL GEOLOGICAL CONTEXT

The southeastern part of the Churchill Province, which formed during the Trans-Hudson orogeny, is linked to two distinct events, namely the New Quebec Orogen in the west and the Torngat Orogen in the east (Wardle et al., 2002). The New Quebec Orogen, active between 1.84 and 1.77 Ga (e.g., Machado et al., 1997; Wardle et al., 2002; Godet et al., 2020 and references therein), comprises a sequence of supracrustal units, in the Labrador Trough, which extends about 850 km from the Ungava Bay in the north to the Grenville Province to the south (Fig. 1; Clark and Wares, 2004).

The Labrador Trough is a geological belt of Proterozoic age (2170–≤1870 Ma) composed primarily of sedimentary and volcanic rocks of the Kaniapiscau Supergroup (Figs. 1, 2) that were emplaced during three distinct cycles of deposition and volcanism, which are separated by erosional unconformities (Clark and Wares, 2004). The simplified stratigraphy of the three cycles is shown in figure 3 and summarized in the following paragraphs.

According to Clark and Wares (2004), the first cycle is composed of an intracratonic rift basin sequence overlain by a passive margin sequence (Fig. 3), which resulted from rifting along the eastern margin of the Archean Superior craton (Figs. 1–3). The rocks of the first cycle are mainly located in the southern part of the belt. Following the deposition of the volcanic and early, immature sedimentary units (base of the first cycle; Seward Group), sandstone, mudstone, and carbonate units (dolomite) (Pistolet Group) were deposited on a passive margin platform. Interpreted to be time-equivalent to the Pistolet Group, the recently recognized Corrugated Hills Continental Flood Basalt records voluminous, plume-related mafic magmatism related to the breakup of the Superior craton at ca. 2171-2166 Ma (van Rooyen et al., 2023). The Pistolet Group is conformably overlain by the Swampy Bay and Attikamagen groups, with the Swampy Bay sequence dated at 2142 Ma (Fig. 3).

An erosional unconformity, representing a period of about 175 million years, separates the rocks of the first and second cycles (Clark and Wares, 2004). The second cycle is characterized by a transgressive sequence (Ferriman Group to the west and Doublet, Koksoak, and LeMoyne groups to the east) composed of platform sedimentary rocks (sandstone and iron formation), including the Baby Formation, one of the main foci of this report, and alkaline volcanic rocks and intrusions (e.g., Nimish volcanic complex and Castignon Complex) (Figs. 2, 3). Towards the end of the second cycle, foundering of the platform was marked by deposition of turbidite and basaltic volcanism (e.g., >1874 ± 3 Ma Hellancourt Formation: Machado et al., 1997).

The ca. 1884–1874 Ma Montagnais sills (Findlay et al., 1995; Machado et al., 1997) are intrusive into rocks of the first and second cycles of the Labrador Trough (Fig. 3) and form part of the Circum-Superior Large Igneous Province (CSLIP), a belt of 1884–1864 Ma mafic–ultramafic rocks that surround much of the Superior craton from the Labrador Trough in the east, the Cape Smith belt and eastern Hudson Bay in the north/northwest, and the Thompson and Fox River belts in the west (Fig. 1; e.g., Ciborowski et al., 2017). In the Labrador Trough, this major magmatic event is thought to also be responsible for 1.88 Ga magmatism of variable composition (felsic and mafic volcanic rocks and carbonatite), including the Nimish, Hellancourt, Willbob, and Douay formations, and the Castignon Lake carbonatite intrusion (e.g., Heaman et al., 2009; Ciborowski et al., 2017). A range of geodynamic settings have been proposed for the origin of the CSLIP, including a deep mantle plume with local evidence for contamination by continental crust (Ciborowski et al., 2017), development of pull-apart basins that formed in a pre-orogen dextral transtensional context (Skulski et al., 1993), formation of back-arc basins during convergence and subduction of Manikewan oceanic crust (e.g., Rohon et al., 1993; Corrigan et al., 2007, 2009), or large-scale passive upwelling of asthenosphere along the already thinned Superior craton margin (Heaman et al., 2009).

The third (and last) cycle of the Kaniapiscau Supergroup is composed of syn-orogenic molasse-type deposits (metapelite, quartzite, calc-silicate rock, sulphide iron formation and silicate iron formation with amphibole), locally intercalated with metabasalt (Chioak and Tamarack River formations; Fig. 3). All units were deformed during the Trans-Hudson orogeny (1845–1783 Ma: Konstantinovskaya et al., 2019). These units now have a dominant NNW-SSE orientation (Fig. 2, Machado et al., 1988).

The rocks of the Labrador Trough are strongly deformed with zones of intense folding and high-strain corridors and major faults. Four deformation events or episodes have been documented (D_1 to D_4: Goulet, 1987; Moorhead, 1989; Moorhead and Hynes, 1990; Wares and Goutier, 1990a; Machado et al., 1997; Konstantinovskaya et al., 2019). D_1 mostly affected sedimentary rocks with a NNW-striking schistosity associated with recumbent, NW-verging folds and local sheath folds. Thrust faults and a decollement fault present at the base of the Hellancourt Formation is associated with D_1, including the Robelin, Archaic, Hérodier, and Garigue faults that represent major fault zones (Fig. 2). D_2 is not developed in the study area, but it is associated with frontal thrust propagation and upright E-NE-trending folds in the Rachel-Laporte and Kuujjuaq zones south-east of the study area (Figs. 2, 4). D_3 is coaxial with D_1 and is associated with the development of NW- to NNW-trending folds and continuation of the deformation front propagation, and with strike-slip shearing. The last episode, D_4, is associated with NE-trending upright folds and normal faults related to exhumation. An axial planar cleavage related to D_4 is locally present where F_3 folds axial orientations are at angle with S4, which created 1-3 type interference patterns (cf. Ramsey, 1967) with F_3 folds.

Economic geology

The Labrador Trough contains syngenetic and diagenetic deposits, including magmatic Cu-Ni-PGE, volcanogenic massive sulphide (VMS), sedimentary exhalative (SEDEX), Mississippi Valley (MVT) Pb-Zn deposits, sedimentary uranium, iron formation, and rare earth elements in carbonatite, and other deposit types. In addition, several epigenetic deposits are related to the movement of hydrothermal fluids during tectonometamorphic events associated with the formation of the New Quebec Orogen.

Clark and Wares (2004) identified a total of 19 different deposit types and more than 336 deposits and showings in the Labrador Trough, many of which consist of iron deposits in large iron formation units. The Koksoak Group, which includes the Baby Formation, hosts SEDEX-type base and precious metal showings and magmatic Cu-Ni-(PGE) and MVT deposits, along with gold vein systems and Ag-Pb-Zn vein deposits in Paleoproterozoic iron-rich units and intrusive rocks.

LOCAL GEOLOGICAL CONTEXT (STUDY AREA)

The earliest geological work in the Labrador Trough was carried out by Albert Peter Low of the Geological Survey of Canada as part of an expedition in 1893 and 1894 (e.g., Low 1896). Since the 1950s, geologists with the governments of Quebec and Canada have carried out geological mapping of the Trough at various scales. The mapping work in the study area was done by Bergeron (1952), Fahrig (1955, 1965), Ciesielski (1975) and Clark (1977, 1978, 1979, 1980). The mining industry also conducted studies during this period. The study area includes a section of the

Baby-Howse and Rachel-Laporte domains (Figs. 2, 4). The latter zone makes up the bulk of the Kan and Willbob properties and includes the Denault Formation (formerly the Abner Formation) of the Attikamagen Group, and the Baby and Hellancourt formations of the Koksoak Group (Fig. 4), all of which are cut by the mafic sills of the Montagnais intrusive suite: Figs. 3, 4).

The Denault Formation, located in the south-central portion of the study area (Fig. 4), consists mainly of dolomite originating from deposition on a regressive passive margin during the first cycle (Clark and Wares, 2004). Although undated, the Denault Formation must be younger than 2142 +4/-2 Ma, the age of rhyolite in the underlying Bacchus Formation of the Swampy Bay Group (Clark, 1984). Farther east, the Robelin thrust fault marks the contact between the Denault Formation and the lower member of the Baby Formation (Fig. 4). Although this contact was documented and described as structural in nature by Dimroth (1970), other authors—including Goulet (1987), Clark (1987) and Wares et al. (1988)—described it as gradual (stratigraphic). Nonetheless, the Robelin fault is still present in the Clark and Wares' (2004) synthesis.

The Baby Formation is subdivided into three members (lower, middle and upper). The lower and upper member comprise mudstone, phyllite, conglomerate, and quartzite, whereas the middle member consists of iron formation and phyllite (Sauvé and Bergeron, 1965). The composition of the banded iron formation in the middle member varies from the base to the top, with oxide facies bands followed by carbonate bands, silicate-carbonate bands and sulphide facies (Clark, 1987). The Hellancourt Formation (Koksoak Group), which overlies the Baby Formation, is characterized by glomeroporphyritic massive and pillowed basalts (Wares and Goutier, 1990a, b; Clark and Wares, 2004). The ca. 1978-1874 Ma Montagnais sills, which are genetically related to the Hellancourt Formation (Wares et al., 1988) and part of the Gerido Intrusive Suite, cut across the rocks of the Baby Formation and are divided into two types: peridotite and massive to subophitic and ophitic gabbro.

The tectonic fabric in the study area is oriented NNW-SSE (Fig. 4), and the axial planes of the folds plunge generally towards the SSE at an average angle of about 15°. Structures associated with the main shortening event (D_1) include folds and various generations of thrust faults, several of which include a dextral strike-slip component (Goulet, 1995). Subsequent NE-SW compression (D_3) produced NE-SW-trending folding and, finally, late NNE-SSW compression (D_4) was associated with the development of a crenulation cleavage, open folds, and extension veins and fractures.

Economic geology of the study area

Early prospecting in the Kan region (Fig. 4) focused primarily on Zn-Cu-Pb massive sulphide-type base metal mineralization. The Koke deposit (1.06 Mt at 6.86% Zn, 1.03% Pb, 0.70% Cu, 54.5 g/t Ag, 1.03 g/t Au) (Armstrong, 1976), located 26 km north of the Kan property, is a typical example of exhalative massive sulphide mineralization. This polymetallic deposit is hosted in a cherty graphitic mudstone unit from the Baby Formation middle member and is likely transitional between Besshi-type volcanogenic deposits and SEDEX-type deposits (Wares et al., 1988).

In the south-central portion of the study area, Pb-Zn veins were discovered in the dolomites of the Denault (Abner) Formation. These mineralized zones are hosted in platform sedimentary rocks

and have characteristics that are similar to those of MVT deposits (Clark and Wares, 2004). The Abner and Riv showings on the Kan property are characterized by centimetre- to decimetre-scale veins and veinlets of sphalerite and galena hosted in dolomitic rocks.

In the late 1980s, exploration for base metals partly transitioned to exploration for precious metals in the Labrador Trough. In 1987, Noranda Exploration ("Noranda") obtained anomalous gold values from a disseminated to massive pyrite-pyrrhotite±arsenopyrite mineralization hosted in carbonate to silicate facies iron formations of the Baby Formation, which became the Dessureault showing. Rio Silver Inc.'s subsequent discovery in 2011 of a major gold showing (Pump Pad Ridge) led to renewed interest in the area for gold exploration. The most distinctive feature of the Pump Pad Ridge showing is the stockwork of quartz-ankerite-chlorite-pyrrhotite veins containing free gold (Hébert and Lee, 2018). The work conducted by Noranda in the 1990s and the early 2000s also confirmed the region's gold potential (Hébert and Lee, 2018). Most of the gold found on O3 Mining Inc.'s Kan property is associated with carbonate facies iron formations in the middle member of the Baby Formation of the Koksoak Group (Figs. 3, 4). In contrast to the Kan property, most showings at the Willbob property consist of gold zones, which are commonly associated with shear zones cutting across mafic to intermediate intrusive rocks of the Montagnais suite such as gabbro, quartz-gabbro, diorite and quartz-diorite (Richard et al., 2018; Richard, 2019). Numerous gold showings have been discovered so far on the Willbob property, as well as some gabbro-hosted Cu-Ni and exhalative Cu-Zn-Co showings, with the earliest discoveries made in the 1950s. Exploration was focussed on base metals in the early years and switched to gold in the late 1980s and early 1990s. Most gold showings consist of shear zone-associated quartz ±ankerite-albite-sulphide fault-fill and extensional-style veins and veinlets and zones of disseminated sulphides. Pyrrhotite is the most common sulphide, with pyrite and locally arsenopyrite. High gold values are commonly associated with arsenopyrite occurrences, although its presence does not systematically correspond to high gold values (Richard et al., 2018; Richard, 2019). The gold zones are generally associated with proximal ankerite, chlorite and albite alteration. One such example of gold mineralization is the Golden Tooth showing (Fig. 4), discovered by Midland Exploration in 2015. The Golden Tooth showing consists of cm- to dm-thick quartz-albite-ankerite veins containing or cut by multiple mm-thick massive arsenopyrite bands in altered (silica, albite, ankerite, and hematite) Montagnais intrusive rocks (Gerido Intrusive Suite; Fig. 4) with disseminated arsenopyrite and pyrite close to the veins (Richard et al., 2018; Richard, 2019). Selected (grab) samples yielded values up to 25 g/t Au, whereas channel sampling gave a value of 1.7 g/t over 3 m. Drilling by Midland Exploration in 2016 intersected gold mineralization at shallow depth, with intervals at 1.12 g/t Au over 3.65 m (including 4.98 g/t Au over 0.5 m), and 1.28 g/t Au over 6.35 m (including 3.81 g/t Au over 0.95 m) (Richard et al., 2018). Most of the vein-style gold mineralized zones in the study area appear to be preferentially associated with folds and structures such as high-strain zones developed in F_4 fold axial planes (Hébert and Lee, 2018). Late D_4 reverse faults associated with back-thrusting control the veins (shear-hosted and fault-fill styles) at many of the showings at the Kan and Willbob properties.

SAMPLE SELECTION AND DESCRIPTION

A series of samples were collected at the Kan and Willbob properties to better characterize the nature of the host rocks, the alteration footprint, and the typology of mineralized zones. Among those samples, two were selected for zircon U-Pb and arsenopyrite Re-Os geochronology (Fig. 4)

to better constrain the age and setting of the gold mineralization in the study area. Although the focus of this report is on the ages obtained, sample description, location, and whole-rock lithogeochemical analyses are provided in Electronic Appendices 1 and 2 for reference.

The Re-Os sample SH-21-32-D from the Willbob property was taken at a depth of 47 m from drill hole WB-16-06 and intersects the Golden Tooth mineralized structure at shallow depth. The sample is part of a mineralized diorite interval that assayed 5.6 g/t Au over 0.45 m, and part of a larger interval that graded 1.3 g/t Au over 6.35 m (Richard et al., 2018). The reported grade of SH-21-32-D is 0.5 g/t Au (Electronic Appendix 2), however because much of the sulphide (arsenopyrite)-rich interval was preserved for Re-Os geochronology, this is considered a lower bound. The subsample used for Re-Os geochronology consists of a quartz-ankerite-feldspar vein containing mm- to cm-thick bands of massive, granoblastic arsenopyrite and finely disseminated arsenopyrite (Fig. 5A, B). The sampled vein is hosted in an ankerite-, chlorite- and albite-altered quartz-diorite (Fig. 5C) and the arsenopyrite crystals are weakly deformed with pressure shadows around granoblastic arsenopyrite (Fig. 5D). Traces of pyrrhotite, sphalerite and free gold are associated with the arsenopyrite, which has been partly recrystallized (Fig. 6A, B).

A sample of polymictic conglomerate (SH-21-15-D) from the lower Baby Formation (Koksoak Group) was taken on the surface in the Noranda Ridge showing area of the Kan property (Fig. 4: sample 21-SH-15; Electronic Appendix 1) to determine the maximum age of deposition of this unit that is at the base of the Koksoak Group and constrain its provenance. The conglomerate is strongly foliated, matrix supported with heterogeneous clast sizes (unsorted to poorly sorted) dominated by rounded cherty clasts and irregular dolomitic clasts (Fig. 7A, B).

ANALYTICAL METHODS AND RESULTS

N-TIMS Re-Os Geochronology Analytical Methods

Preparation of an arsenopyrite mineral separate from SH-21-32-D was made by metal-free crushing and milling coupled with magnetic and gravity mineral separation techniques. The mineral separate was initially analyzed for Re content by semi-quantitative methods to evaluate its viability for Re-Os dating. The ^{187}Re and ^{187}Os concentrations were determined using isotope dilution and negative thermal ionization mass spectrometry (N-TIMS) techniques at the University of Alberta. Preliminary Re-Os analysis established that Re concentrations were ~90 ppb and that the Os present in SH-21-32D was >99.5% radiogenic Os (i.e. ^{187}Os*) and therefore effectively devoid of common Os. Therefore, Re-Os ages are more accurately determined using a mixed double-Os spike containing ^{185}Re + ^{188}Os + ^{190}Os, which allows for accurate mass bias corrections on Os (Markey et al., 2003, 2007). Spiked samples were dissolved at 220˚C for 48 hours, followed by chemical separation and purification of Os and Re using procedures described in Shirey and Walker (1995), Cohen and Waters (1996), and Birck et al. (1997), and explained in detail in Morelli et al. (2005). Isotopic measurements were collected in static mode using faraday cups on a ThermoScientific Triton mass spectrometer. Total procedural blanks before these analyses were <3 picograms Re and ≤0.1 picograms Os (<0.01 picogram ^{187}Os). The Reference Material 8599 Henderson molybdenite (Markey et al., 2007) is routinely analyzed as a standard, and during the past 5 years returned an average Re-Os date of 27.78 ± 0.06 Ma (n= 18), indistinguishable from the Reference Age Value of 27.66 ± 0.1 Ma (Wise and Watters, 2011). The ^{187}Re decay constant

(λ^{187}Re) used for age calculation is 1.666 ± 0.005 x10^{-11} a^{-1} (Smoliar et al., 1996), a value which is cross-calibrated to the U-Pb system (^{238}U and ^{235}U) to better than ~ ± 0.31% (Selby et al., 2007).

Re-Os Analytical Results

The results of the Re-Os age determinations are presented in Table 1. The age uncertainty is quoted at 2σ level, and includes all known analytical uncertainty, including a ~0.31% uncertainty in the decay constant of ^{187}Re. Three analyses of SH-21-32-D yield a weighted average model age of 1810.7 ± 4.6 Ma (Table 1, Fig. 8).

SHRIMP U-Pb Zircon Geochronology Analytical Methods

The Kan polymictic conglomerate sample SH-21-15-D was processed at the Geochronology facility of the Geological Survey of Canada (GSC; Ottawa, Ontario) using standard crushing, grinding, Wilfley™ table, and magnetic and heavy-liquid separation methods. Sensitive high-resolution ion microprobe (SHRIMP) U-Pb geochronological analyses were conducted using the SHRIMP II instrument at the J.C. Roddick Ion Microprobe facility at the GSC (Ottawa, Ontario), following the analytical procedures of Stern (1997) and Stern and Amelin (2003). To ensure a robust detrital zircon age distribution, zircon grains were selected as randomly as possible to minimize any bias in the picking process. The grains were mounted in a 2.5 cm diameter epoxy mount together with reference materials. Zircon z6266 was used as the primary reference material (^{206}Pb/^{238}U age = 559 Ma; Stern and Amelin, 2003) and zircon z1242 as the secondary reference material (^{207}Pb/^{206}Pb age = 2679.7 Ma; Davis et al., 2019). Both reference materials were analysed on the same mount and under the same conditions as the unknowns. Using a spot size of ~16 μm and a 16O- primary current of 8 nA, each SHRIMP analysis involved a set of 6 scans over 11 isotope masses of Zr^+, U^+, Pb^+, Th^+, Yb^+, and Hf^+. The data was processed offline using SQUID3 software (Bodorkos et al., 2020). Analyses of the secondary reference material z1242 were interspersed between the sample analyses to monitor accuracy of the measured ^{207}Pb/^{206}Pb ratios and to correct for any instrumental mass bias. No fractionation was observed and no correction needed to be applied to the Pb-isotope data. The Pb composition of the surface blank was used to correct for ^{204}Pb, following the methods of Stern (1997). The SHRIMP U-Pb results and further details of analytical conditions during the session (e.g., mount number, spot size, primary beam intensity etc.) are provided in Electronic Appendices 3 and 4, respectively. Errors reported in Electronic Appendix 3 are given at the 1σ confidence interval.

ID-TIMS U-Pb Zircon Geochronology Analytical Methods

Isotope dilution thermal ionization mass spectrometry (ID-TIMS) analyses were performed at the GSC on zircons separated from sample SH-21-15-D. Prior to ID-TIMS, all grains were chemically abraded (Mattinson, 2005) using concentrated hydrofluoric acid (HF) at 190°C for 15 hours after they were annealed at 900°C for 48 hours. The ID-TIMS analytical methods applied here follows the method of Parrish et al. (1987) but is modified through the addition of an in-house ^{205}Pb–^{233}U–^{235}U spike and analysis on a Triton thermal ionization mass spectrometer. All common Pb for the zircon analyses was attributed to the procedural blank (~0.3–0.7 pg) and assigned the long-term isotopic composition of the laboratory's procedural blank. The U-blank was corrected using a value of ≤0.1 pg. Isotope measurements were processed using the TRIPOLI software package

(Bowring et al., 2011). Data reduction and error propagation were done using the program ET_Redux and related algorithms (McLean et al., 2011). U-Pb ID-TIMS analytical results are presented in Electronic Appendix 5 and data reduction parameters are given in Electronic Appendix 6. All uncertainties are reported at 2σ in Electronic Appendix 5.

For both SHRIMP and TIMS results, Isoplot v. 4.15 (Ludwig, 2012) was used to generate concordia plots and calculate weighted means. Ages were calculated using the decay constants and natural $^{238}U/^{235}U$ ratio (137.88) recommended by Steiger and Jäger (1977). The error ellipses on the concordia diagram (Fig. 9) and the weighted mean errors in the text are reported at the 95% confidence level. The probability density diagram was generated using AgeDisplay (Sircombe 2004).

U-Pb Analytical Results

Zircon recovered from sample SH-21-15-D occurs as colourless to pale brown, subhedral or rounded prismatic to equant crystals, ~75–200 μm in length (Fig. 9A inset). CL images reveal variable zoning patterns in zircon interiors, including oscillatory, sector, fir-tree, or irregular zoning. Many crystals have outer, dark or less commonly bright rims of variable thickness that surround or transect the zoned interiors. The rims are either homogeneous or zoned.

Ninety-one SHRIMP analyses were conducted across 83 zircon crystals, with $^{207}Pb/^{206}Pb$ dates ranging between ca. 2853 and 2545 Ma (Fig. 9; Electronic Appendix 3). Replicate analyses were made on 4 of the youngest grains, with grain 100 giving the best results with a weighted mean age of 2619 ± 11 Ma (n = 3; MSWD = 0.42). This age is considered as the best estimate for the maximum age of deposition for the conglomerate. The replicate analyses from the other 3 grains yielded non-reproducible results attributed to the effects of variable Pb loss. On a combined probability density distribution and histogram plot (Fig. 9B), the data display a dominant mode at 2695 Ma, as well as smaller ones at 2850, 2795, 2640, and 2620 Ma.

Four additional zircon grains, prismatic in shape, were analyzed by ID-TIMS, all of which are concordant to sub-concordant with $^{207}Pb/^{206}Pb$ dates ranging between 2738.0 ± 1.4 and 2705.1 ± 1.5 Ma (Fig. 9C; Electronic Appendix 5). All these dates fall within the dominant age mode defined by the SHRIMP data.

CONSTRAINTS ON THE TIMING OF GOLD MINERALIZATION

The 1810.7 ± 4.6 Ma weighted mean Re-Os age obtained on gold-bearing arsenopyrite from a mineralized vein at the Golden Tooth prospect of the Willbob property is the first direct dating of gold mineralization in the Labrador Trough. It is interpreted as the age of structurally controlled, quartz-diorite-hosted vein-style gold mineralization in the northern part of the Trough. This indicates a mineralizing event approximately 60 to 75 million years after the emplacement of the Montagnais intrusive rocks, which have been dated at 1884.0 ± 1.6 Ma and at 1874 ± 3 Ma (Findlay et al., 1995; Machado et al., 1997) and are coeval with cycle 2 of the Labrador Trough stratigraphy. This dated phase of gold mineralization was roughly synchronous with regional metamorphism and subsequent cooling in the New Quebec Orogen dated between ca. 1840 and 1770 Ma (Godet et al., 2020 and references cited in their Table 1). At the Golden Tooth showing, the mineralized

veins are compatible with D_4 deformation and the associated fabrics as the veins are preferentially developed in F_4 axial planar zones at the intersection of folded S_0 surfaces, suggesting that the veins are relatively late in the tectonic evolution of the area. Interestingly, the 1811 Ma arsenopyrite Re-Os age is similar to the age of an undeformed (late- to post-tectonic) monzonitic intrusion (1813 Ma) in the central sector of the orogen (Machado et al., 1997), suggesting a temporal association between orogenic auriferous hydrothermal activity and felsic magmatism at belt scale. At a larger scale, the Trans-Hudson Orogen represents an important metallotect for gold as shown in central and northern Canada (e.g., Lynn Lake, Manitoba: Lawley et al., 2020; Snow Lake, Manitoba: Rubingh et al., 2024; Meliadine, Nunavut: Carpenter et al., 2005; Lawley et al., 2015; and Meadowbank: Janvier et al., 2015), and the new Re-Os age presented herein indicates that this orogen was also responsible for orogenic-style gold mineralization in the Labrador Trough.

The youngest detrital zircon grain dated in this study for the Kan polymictic conglomerate provides a maximum age of deposition of ≤2619 ± 11 Ma for the lower member of the Baby Formation, whereas the ca. 1884–1874 Ma Montagnais sills, which crosscut units of cycles 1 and 2 (Fig. 3), provide a minimum age constraint on deposition. Although the absence of Paleoproterozoic detrital zircon makes it difficult to constrain its age more accurately, the presence of large, abundant, and irregular limestone clasts as well as abundant, rounded chert clasts in the conglomerate, both of which are most likely sourced from underlying units in the region such as the Denault (or Abner) Formation, suggests that it was deposited post-ca. 2142 Ma. The Archean detritus in the Kan conglomerate, of ca. 2850, 2795, 2738-2705, 2695, 2640, and 2620 Ma age based on the combined SHRIMP and ID-TIMS results, is consistent with derivation from the northeastern Superior Province, such as the ≤2.88 Ga Rivière-Arnaud terrane (e.g., Percival et al., 2012). Alternatively, or in addition, the Archean detritus could reflect recycling of cycle 1 sedimentary rocks. Thus, the detrital age data, combined with the nature and composition of clasts in the conglomerate, indicate that the source of sediments in the Baby Formation conglomerate comprises mixed Archean zircon material and Proterozoic chemical sedimentary rocks. Henrique-Pinto et al. (2017b) dated three sandstone samples from the Baby Formation, which also contain detrital zircon exclusively of Archean age (3.06, 2.94–2.80, 2.72, 2.70 Ga), and identified the Superior craton as the main source of sediments. The absence of ca. 1.88 Ga detritus in the dated conglomerate suggests that it was deposited early during cycle 2 sedimentation, prior to ca. <1874 Ma mafic volcanism (Hellancourt Formation), in a divergent setting (e.g., Henrique-Pinto et al., 2017b). More work would be necessary to better constrain the depositional age of sedimentary units in the Kan property, and by extension the timing of gold introduction, such as dating turbidite deposited contemporaneously with Hellancourt basalt.

ACKNOWLEDGMENTS

This study is part of the "*OS-3 – Orogenic gold deposits: A closer look at the diversity of types, styles and ages of gold deposits in greenstone belts*" project of the Targeted Geoscience Initiative Program of the Geological Survey of Canada and includes an MSc project by S. Hébert conducted at the Institut national de la recherche scientifique, Centre Eau Terre Environnement. PML sincerely acknowledges A.-A. Sappin and D. Corrigan for generously agreeing to share some of their figures of the Trans-Hudson Orogen and Labrador Trough. M. Boutin helped with preparing some figures. The authors are most grateful to Exploration Midland, Minière O3, and Les

Ressources Tectonic for access to samples and data and for scientific support. The staff of the Geochronology Laboratories at the Geological Survey of Canada are thanked for their careful efforts and excellent work in preparing high-quality mineral separates (R. Chung, G. Case, and Q. Emon), generating the high-precision U–Pb ID–TIMS data (J. Peressini and C. Lafontaine), and producing the ion probe mount and SHRIMP instrument tuning and troubleshooting (T. Pestaj). M. Polivchuk (GSC) provided high-quality scanning electron microscope images for targeting SHRIMP analytical sites. Thanks to S. Trépanier, L.-P. Richard, P. Simard, C. Lee, S. Houle, N. Rosengren, and B. Dubé for insightful discussions on the geology of the Willbob and Kan exploration projects and on gold deposits in general. Thanks to D. Hnatyshin for his constructive review of the manuscript.

REFERENCES

Armstrong, R.C., 1976, Koke Project: Cominco, Statutory work report submitted to Ministère des Richesses naturelles, GM 32180, 70 p.

Bergeron, R., 1952, Geology of Forbes Lake Area, Ungava: Unpublished M.Sc. thesis, Columbia University, New-York, United States of America, 99 p.

Birck, J.L., Roy Barman, M., and Capmas, F., 1997, Re-Os isotopic measurements at the femtomole level in natural samples: Geostandards Newsletter, v. 20, p. 19–27.

Bodorkos, S., Bowring, J.F., and Rayner, N.M., 2020, Squid3: Next-generation data processing software for Sensitive High Resolution Ion Micro Probe (SHRIMP); *in* Exploring for the Future, (eds.) Czarnota, K., Roach, I., Abbott, S., Haynes, M., Kositcin, N., Ray, A. and Slatter, E.; Extended Abstracts, Geoscience Australia, Canberra, p. 1–4.

Bowring, J., McLean, N.M., and Bowring, S., 2011, Engineering cyber infrastructure for U-Pb geochronology: TRIPOLI and U-Pb_Redux: Geochemistry, Geophysics, Geosystems, v. 12: Q0AA19.

Carpenter, R.L., Duke, N.A., Sandeman, H.A., and Stern, R., 2005, Relative and absolute timing of gold mineralization along the Meliadine trend, Nunavut, Canada: Evidence for Paleoproterozoic gold hosted in an Archean greenstone belt: Economic Geology, v. 100, p. 567–576.

Ciborowski, T.J.R., Minifie, M.J., Kerr, A.C., Ernst, R.E., Baragar, B., Millar, I.L., 2017, A mantle plume origin for the Palaeoproterozoic Circum-Superior Large Igneous Province: Precambrian Research, v. 294, p. 189–213.

Ciesielski, A., 1975, Contact Archéen-Protérozoïque entre les lacs Forbes et Sénat (Fosse du Labrador. Ministère des Richesses naturelles, DPV 449, 24 p.

Clark, T., 1977, Geology of the Forbes Lake Area, New Quebec Territory: Ministère des Richesses naturelles, Preliminary report DPV 452, 13 p., 1 map.

Clark, T., 1978, Région du lac Hérodier, Nouveau-Québec, Canada: Ministère des Richesses naturelles, Rapport préliminaire, DPV 568, 34 p., 2 maps.

Clark, T., 1979, Région du lac Napier, Nouveau-Québec, Canada: Ministère des Richesses naturelles, Rapport préliminaire, DPV 663, 18 p., 1 map.

Clark, T., 1980, Région de la rivière Koksoak, Nouveau-Québec, Canada: Ministère de l'Énergie et des Ressources, Rapport préliminaire, DPV-781, 14 p., 1 map.

Clark, T., 1984, Géologie de la région du lac Cambrien, Territoire du Nouveau-Québec: Ministère de 1'Énergie et des Ressources, Québec, ET 83-02.

Clark, T., 1987, Stratigraphie, pétrographie et pétrochimie de la formation de fer de Baby dans la région de lac Hérodier (Fosse du Labrador): Ministère de l'Énergie et des Ressources, ET 87-13, 44 p.

Clark, T. and Wares, R., 2004, Synthèse lithotectonique et métallogénique de l'Orogène de Nouveau-Québec (Fosse du Labrador): Ministère des Ressources naturelles, de la Faune et des Parcs, MM 2004-01, 176 p.

Cohen, A.S., and Waters, F.G., 1996, Separation of osmium from geological materials by solvent extraction for analysis by thermal ionization mass spectrometry: Analytica Chimica Acta, v. 332, p. 269–275.

Corrigan, D., Galley, A.G., and Pehrsson, S., 2007, Tectonic evolution and metallogeny of the Southwestern Trans-Hudson orogen: Geological Association of Canada, Mineral Deposits Division, Special Publication 5, p. 881–902.

Corrigan, D., Pehrsson, S., Wodicka, N., and de Kemp, E., 2009, The Paleoproterozoic Trans-Hudson Orogen: a prototype of modern accretionary processes: Geological Society, London, Special Publications, v. 327, p. 457−479.

Corrigan, D., van Rooyen, D., and Wodicka, N., 2021, Indenter tectonics in the Canadian Shield: A case study for Paleoproterozoic lower crust exhumation, orocline development, and lateral extrusion: Precambrian Research, v. 355, paper 106083.

Corriveau, L., 2007, Iron oxide copper-gold deposits: A Canadian perspective: Geological Association of Canada, Mineral Deposits Division, Special Publication 5, p. 307–328.

Davis, W.J., Pestaj, T., Rayner, N., and McNicoll, V.M., 2019, Long-term reproducibility of $^{207}Pb/^{206}Pb$ age at the GSC SHRIMP lab based on the GSC Archean reference zircon z1242: Geological Survey of Canada, Scientific Presentation 111, 1 poster.

Dimroth, E., 1970, Evolution of the Labrador geosyncline: Geological Society of America Bulletin, v. 81, p. 2717–2742.

Fahrig, W.F., 1955, Lac Herodier, New Quebec (Preliminary Map and Descriptive Notes): Geological Survey of Canada, Paper 55-1, 9 p., 1 map.

Fahrig, W.R., 1965, Geology, Lac Herodier, Québec: Geological Survey of Canada, A Series Map 1146A, 1 sheet.

Findlay, J.M., Parrish, R.R., Birkett, T.C., and Watanabe, D.H., 1995, U-Pb ages from the Nimish Formation and Montagnais glomeroporphyritic gabbro of the central New Quebec Orogen, Canada: Canadian Journal of Earth Sciences, v. 32, p. 1208–1220.

Galley, A.G., Syme, R., and Bailes, A.H., 2007, Metallogeny of the Paleoproterozoic Flin Flon belt, Manitoba and Saskatchewan: Geological Association of Canada, Mineral Deposits Division, Special Publication 5, p. 509–531.

Godet, A., Guilmette, C., Labrousse, L., Smit, M., Davis, D.W., Raimondo, T., Vanier, M.-A., Charette, B., and Lafrance, I., 2020, Contrasting P-T-t paths reveal a metamorphic discontinuity in the New Quebec Orogen: Insights into Paleoproterozoic orogenic processes: Precambrian Research, v. 342, paper 105675.

Goulet, N., 1987, Étude tectonique de la partie nord de la Fosse du Labrador: Ministère de l'Énergie et des Ressources, MB 87-21, 33 p.

Goulet, N., 1995, Étude structurale, stratigraphique et géochronologique de la partie nord de la Fosse du Labrador: Ministère des Ressources naturelles, MB 95-36, 35 p.

Gross, G.A., 1993, Industrial and genetic models for iron ore in iron-formations: Geological Association of Canada, Special Paper 40, p. 151–170.

Heaman, L.M., Peck, D., and Toope, K., 2009, Timing and geochemistry of 1.88 Ga Molson Igneous Events, Manitoba: insights into the formation of a craton-scale magmatic and metallogenic province: Precambrian Research, v. 172, p. 143–162.

Hébert S., and Lee C., 2018, Technical Report 2018 Exploration Program Kan Project, Labrador Trough, Québec: Osisko Mining Inc., Statutory work report submitted to Ministère des Ressources naturelles, GM 71136, 1828 p.

Henrique-Pinto, R., Guilmette, C., Bilodeau, C., McNicoll, V., and Corrigan, D., 2017a, Analyse de la provenance sédimentaire dans le nord de la Fosse du Labrador, Nunavik-Québec : contraintes pétrographiques et géochronologiques: Ministère des Ressources naturelles, MB 2017-09, 23 p.

Henrique-Pinto, R., Guilmette, C., Bilodeau, C., and McNicoll, V., 2017b, Evidence for transition from a continental forearc to a collisional pro-foreland basin in the eastern Trans-Hudson orogen: detrital zircon provenance analysis in the Labrador Trough, Canada: Precambrian Research, 296: 181–194.

Hoffman, P., 1988, United plates of America, the birth of a craton: Early Proterozoic assembly and growth of Proto-Laurentia: Annual Reviews of Earth and Planetary Science, v. 16, p. 543–603.

Janvier, V., Castonguay, S., Mercier-Langevin, P., Dubé, B., Malo, M., McNicoll, V.J., Creaser, R.A., de Chavigny, B., and Pehrsson, S.J., 2015, Geology of the banded iron formation-hosted Meadowbank gold deposit, Churchill Province, Nunavut: Geological Survey of Canada Open File 7852, p. 255–269.

Konstantinovskaya, E., Ivanov, G., Feybesse, J.-L., and Lescuyer, J.-L., 2019, Structural features of the central Labrador Trough: A model for strain partitioning, differential exhumation and late normal faulting in a thrust wedge under oblique shortening: Geoscience Canada, v. 46, p. 5–30.

Lafrance, I., Bandyayera, D., Simard, M., 2012, Géologie – Ile Koksoak: Ministère des Ressources naturelles et de la Faune, map CG-24F11-2012-01, scale 1 : 50 000.

Lawley, C.J.M., Creaser, R.A., Jackson, S., Yang, Z., Davis, B., Pehrsson, S., Dubé, B., Mercier-Langevin, P., and Vaillancourt, D., 2015, Unraveling the Western Churchill Province Paleoproterozoic gold metallotect: constraints from Re-Os arsenopyrite and U-Pb xenotime geochronology and LA-ICP-MS arsenopyrite trace element chemistry at the BIF-hosted Meliadine gold district, Nunavut, Canada: Economic Geology, v. 110, p. 1425–1454.

Lawley, C.J.M., Selby, D., Davis, W.J., Yang, E., Zhang, S., Jackson, S.E., Petts, D.C., O'Connor, A.R., and Schneider, D.A., 2020, Paleoproterozoic gold and its tectonic triggers and traps: Implications from Re-Os sulphide and U-Pb detrital zircon geochronology, Lynn Lake, Manitoba: Geological Survey of Canada, Open File 8712, p. 211–222.

Layton-Matthews, D., Lesher, M., Burnham, O.M., Liwiang, J., Halden, N.M., Hulbert, L., and Peck, D.C., 2007, Magmatic Ni-Cu-platinum-group element deposits of the Thompson Nickel belt: Geological Association of Canada, Mineral Deposits Division, Special Publication 5, p. 409–432.

Lesher, C.M., 2007, Ni-Cu-(PGE) deposits in the Raglan area, Cape Smith belt, New Quebec: Geological Association of Canada, Mineral Deposits Division, Special Publication 5, p. 351–386.

Low, A.P., 1896, Report on the exploration in the Labrador Peninsula along the east Main, Koksoak, Hamilton, Manicuagan and portions of other rivers in 1892-93-94-95: Geological Survey of Canada, Annual Report (1995), 387 p.

Ludwig, K.R., 2012, Isoplot 4.75: A geochronological toolkit for Microsoft Excel: Berkeley Geochronology Center, Special Publication 5, 75 p.

Machado, N., Perreault, S., and Hynes, A., 1988, Timing of continental collision in the Northern Labrador Trough, Quebec: evidence from U-Pb geochronology: Geological Association of Canada – Mineralogical Association of Canada, Program with Abstracts v. 13, p. A76.

Machado, N., Clark, T., David, J., and Goulet, N., 1997, U-Pb ages for magmatism and deformation in the New Quebec orogen: Canadian Journal Earth Sciences, v. 34, p. 716–723.

Markey, R., Hannah, J.L., Morgan, J.S.W., and Stein, H.J., 2003, A double spike for osmium analysis of highly radiogenic samples: Chemical Geology, v. 200, p. 395–406.

Markey, R., Stein, H.J., Hannah, J.L., Selby, D., and Creaser, R.A., 2007, Standardizing Re-Os geochronology: A new molybdenite Reference Material (Henderson, USA) and the stoichiometry of Os salts: Chemical Geology, v. 244, p. 74–87.

Mattinson, J. M., 2005, Zircon U–Pb chemical abrasion ("CA-TIMS") method: Combined annealing and multi-step partial dissolution analysis for improved precision and accuracy of zircon ages: Chemical Geology, v. 220, p. 47–66.

McLean, N.M., Bowring, J.F., and Bowring, S.A., 2011, An algorithm for U-Pb isotope dilution data reduction and uncertainty propagation: Geochemistry, Geophysics, Geosystems, v. 12: Q0AA18.

Moorhead, J., 1989, Géologie de la région du lac Chukotat (Fosse de l'Ungava): Ministère de l'Énergie et des Ressources, ET 87-10, 56 p.

Moorhead, J., and Hynes, A., 1990, Nappes in the internal zone of the northern Labrador Trough: Evidence for major early, NW-vergent basement transport: Geoscience Canada, v. 17, p. 241–244.

Morelli, R.M., Creaser, R.A., Selby, D.J., Kontak, D.J., and Horne, R.J., 2005, Rhenium-osmium arsenopyrite geochronology of Meguma group gold deposits, Meguma Terranne, Nova Scotia, Canada: evidence for multiple gold mineralizing events: Economic Geology, v. 100, p. 1229–1242.

Parrish, R.R., Roddick, J.C., Loveridge, W.D., and Sullivan, R.W., 1987, Uranium-lead analytical techniques at the Geochronology Laboratory, Geological Survey of Canada: Geological Survey of Canada, Paper 87-2, p. 3-7.

Percival, J., Skulski, T., Sanborn-Barrie, M., Stott, G., Leclair, A.D., Corkery, M.T., and Boily, M., 2012, Geology and tectonic evolution of the Superior Province, Canada; *in* Tectonic Styles in Canada: The Lithoprobe Perspective, (eds.) J. Percival, F. Cook, and R. Clowes; Geological Association of Canada Special Paper, v. 49, p. 321–378.

Ramsey, J.G., 1967, Folding and fracturing of rocks: McGraw-Hill, New York, 568 p.

Richard, L.-P., Bourrassa, S., and Bédard, F., 2018, 2016-2017 prospection and drilling campaigns, JULY 2018 prospection campaign, Wilbob project, Labrador Trough, NTS 24K04, 24F13, 24F14, 24F12, 24F11, 24F06, 24F07, 24F02: Midland Exploration, Statutory work report submitted to Ministère de l'Énergie et des Ressources naturelles, GM 71411, 1464 p.

Richard, L.-P., 2019, 2018 trenching and channel sampling, Willbob Project, Labrador Trough NTS 24K04, 24F13, 24F14, 24F12, 24F11, 24F06, 24F07, 24F02: Midland Exploration, Statutory

work report submitted to Ministère de de l'Énergie et des Ressources naturelles, GM 71491, 289 p.

Rohon, M.-L., Vialette, Y., Clark, T., Roger, G., Ohnenstetter, D., and Vidal, P., 1993, Aphebian mafic-ultramafic magmatism in the Labrador Trough (New Quebec): Canadian Journal of Earth Sciences, v. 30, p. 1582–1593.

Rubingh, K.E.L., Lafrance, B., and Gibson, H.L., 2024, The Snow Lake deposits in Manitoba, Canada: Formation of metamorphosed amphibolite facies orogenic gold deposits during a progressive and prograde orogenic event: Economic Geology, v. 119, p. 421–444.

Sappin, A.-A., Houlé, M.G., Corrigan, D., Bédard, M.-P., Rayner, N., Wodicka, N., and Brind'Amour-Côté, C., 2022, Petrography, chemical composition, and age constraints of mafic intrusions from the Mesoproterozoic Soisson Intrusive Suite in the southeastern Churchill Province (Canada): Canadian Journal of Earth Sciences, v. 59, p.189–204.

Sauvé, P., and Bergeron, R., 1965, Région des lacs Gérido et Thévenet, Nouveau-Québec: Ministère des Richesses naturelles du Québec, RG 104, 109 p., 3 maps.

Selby, D., Creaser, R.A., Stein, H.J., Markey, R.J., and Hannah, J.L., 2007, Assessment of the ^{187}Re decay constant by cross calibration of Re–Os molybdenite and U–Pb zircon chronometers in magmatic ore systems: Geochimica et Cosmochimica Acta, v. 71, p. 1999–2013.

Shirey, S.B., and Walker, R.J., 1995, Carius tube digestion for low blank Re-Os analysis: Anal. Chem., v. 67, p. 2136–2141.

Sircombe, K.N., 2004, AGEDISPLAY: an Excel workbook to evaluate and display univariate geochronological data using binned frequency histograms and probability density distributions: Computers and Geosciences, v. 30, p. 21–31.

Skulski, T., Wares, P.R., and Smith, A.D., 1993, Early Proterozoic (1.88-1.87 Ga) tholeiitic magmatism in the New Québec orogen: Canadian Journal of Earth Science, v. 30, p. 1505–1520.

Smoliar, M.I., Walker, R.J., and Morgan, J.W., 1996, Re-Os ages of group IIA, IIIA, IVA, IVB iron meteorites: Science, v. 271, p. 1099–1102.

Steiger, R.H., and Jäger, E., 1977, Subcommission on geochronology: Convention on the use of decay constants in geo-and cosmochronology: Earth and Planetary Science Letters, v. 36, p. 359–362.

Stern, R.A., 1997, The GSC Sensitive High Resolution Ion Microprobe (SHRIMP): Analytical techniques of zircon U–Th–Pb age determinations and performance evaluation: Geological Survey of Canada, Current Research 1997-F, p. 1–31.

Stern, R.A., and Amelin, Y., 2003, Assessment of errors in SIMS zircon U–Pb geochronology using a natural zircon standard and NIST SRM 610 glass: Chemical Geology, v. 197, p. 111–146.

Trepanier S., and Dessureault, M., 2000, Propriété Kan, Fosse du Labrador: Noranda Inc. Exploration, Statutory work report : Ministère des Ressources naturelles, GM 58601, 409 p.

Valette, M., Mercier-Langevin, P., De Souza. S, Bécu, V., Lauzière, K., and Côté-Mantha, O., 2023, Whole-rock lithogeochemistry of the Amaruq orogenic gold deposit, western Churchill Province, Nunavut: Geological Survey of Canada, Open File 8973, 1 .zip file.

Van Rooyen, D., Sappin, A.-A., Corrigan, D., Rayner, N., and Houlé, M.G., 2023, The Corrugated Hills Continental Flood Basalt: a c. 2.17 Ga flood basalt province related to breakup of the Superior craton; *in* Supercontinents, Orogenesis and Magmatism, (eds.) R.D. Nance, R.A. Strachan, C. Quesada, and S. Lin; Special Publication of the Geological Society of London, v. 542, https://doi.org/10.1144/SP542-2023-19

Wardle, R.J., James, D.T., Scott, D.J., and Hall, J., 2002, The southeastern Churchill Province: synthesis of a Paleoproterozoic transpressional orogen: Canadian Journal of Earth Sciences, v. 39, p. 639–663.

Wares, R., Berger, J., and St-Seymour, K., 1988, Synthèse métallogénique des indices de sulfures au nord du 57 parallèle, Fosse du Labrador (rapport intérimaire : étape I): Ministère de l'Énergie et des Ressources, MB 88-05, 186 p.

Wares, R.P., and Goutier, J., 1990a, Deformational style in the foreland of the northern New Québec orogen: Geoscience Canada, v. 17, p. 244–249.

Wares, R., and Goutier J., 1990b, Synthèse métallogénique des indices de sulfures au nord du 57e parallèle, Fosse du Labrador (rapport intérimaire : étape III): Ministère de l'Énergie et des Ressources, MB 90-25, 82 p., 2 maps.

Wise, S.A., and Waters, R.L., 2011, Reference material 8599 Henderson molybdenite: National Institute of Standards and Technology Report of Investigation, 30 March 2011.

Table 1. Re-Os arsenopyrite data.

Sample	Aliquot	weight (g)	Re (ppb)	± 2σ	^{187}Re (ppb)	± 2σ	^{187}Os (ppb)	± 2σ	Model Age (Ma)[1]	± 2σ
SH-21-32-D	MD	0.09971	0.1086	0.0003	68.270517	0.190807	2.094796	0.002503	1814.1	7.9
SH-21-32-D	MD-R1	0.21508	0.1119	0.0003	70.362985	0.196507	2.154508	0.004244	1810.4	8.4
SH-21-32-D	MD-R2	0.19745	0.1104	0.0003	69.395257	0.193838	2.121083	0.003965	1807.2	8.3

[1]Model ages are based on the isotope equation [$t = \ln(^{187}Os_{radiogenic}/^{187}Re + 1) / \lambda$; where t = model age and $\lambda = 1.666 \times 10^{-11}$] using an assumed mantle-like $^{187}Os/^{188}Os$ initial at 0.5. Model ages are for reference only (see text for further discussion)

Analyses conducted using a mixed double-Os tracer solution of $^{185}Re + ^{188}Os + ^{190}Os$; analytical uncertainties are reported at 2σ; all data are blank corrected

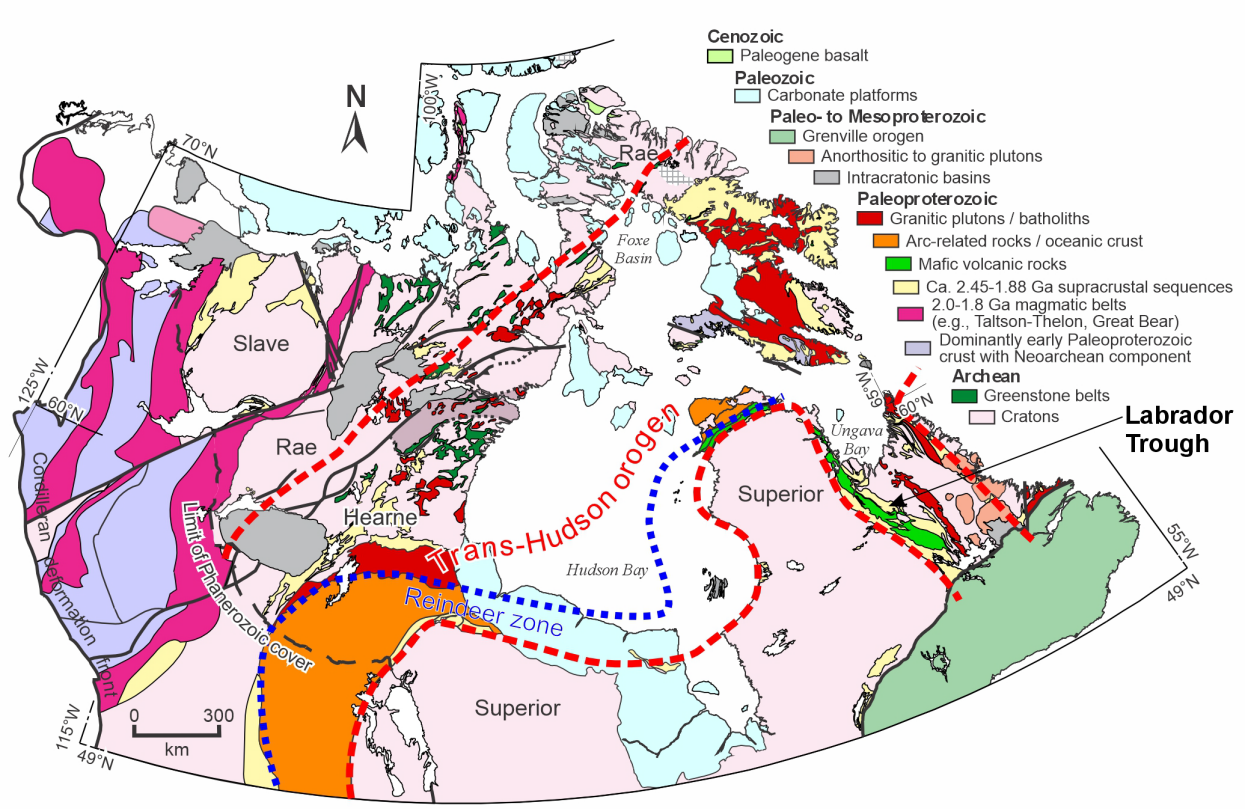

Figure 1. Simplified geological map of the Canadian Shield (from Corrigan et al., 2009), with extension of western Precambrian terranes shown beneath Phanerozoic cover. Minimum limit of Trans-Hudson age tectono-thermal overprint (1.83-1.80 Ga) is shown by the thick red dashed lines. Limit of the Reindeer Zone is shown (thick stippled blue line).

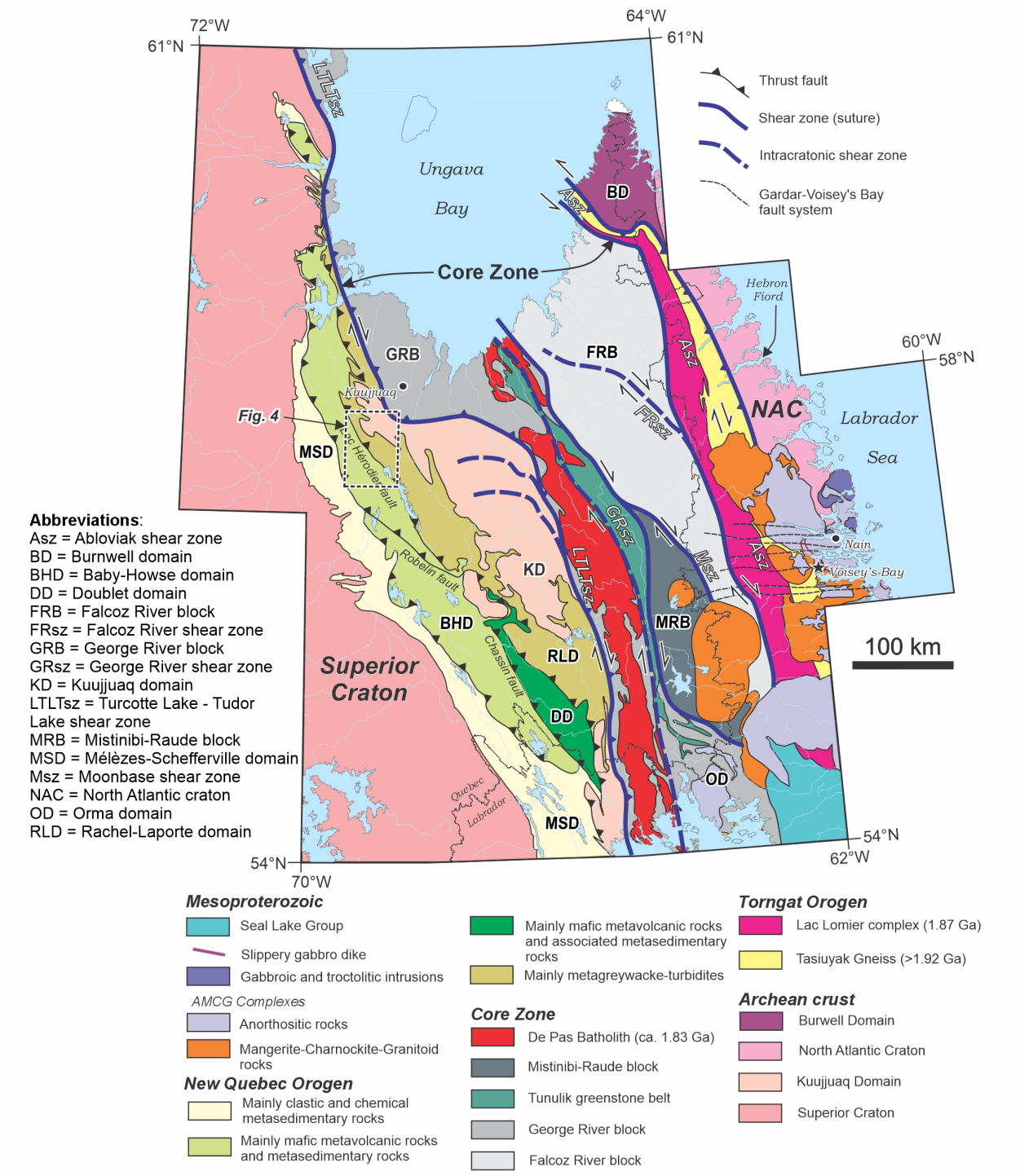

Figure 2. Simplified geological map of the southeastern part of the Churchill Province showing the main lithotectonic divisions and the principal faults and high strain corridors of the New Quebec Orogen (Taken from Corrigan et al., 2021, and Sappin et al., 2022). Also shown is the location of the study area.

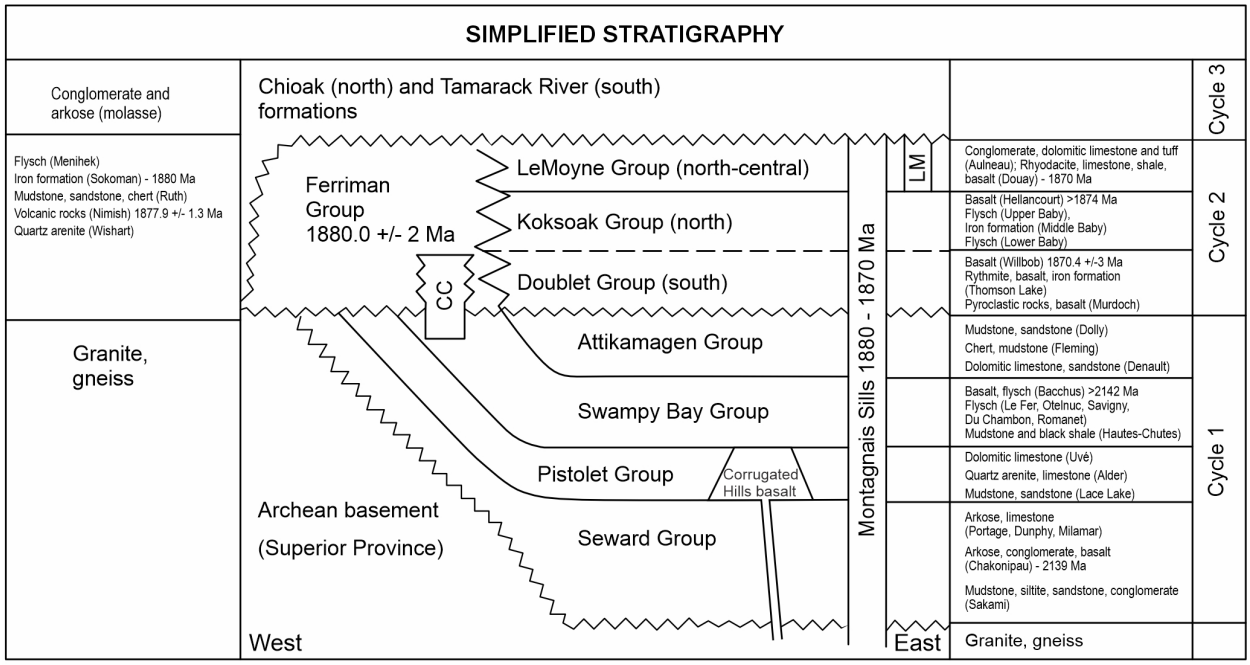

Figure 3. Simplified stratigraphy of the Labrador Trough, Kaniapiscau Supergroup. Modified from Clark and Wares (2004), Henrique-Pinto et al. (2017a) and van Rooyen et al. (2023). Abbreviations: CC = Castignon complex, LM = LeMoyne carbonatite.

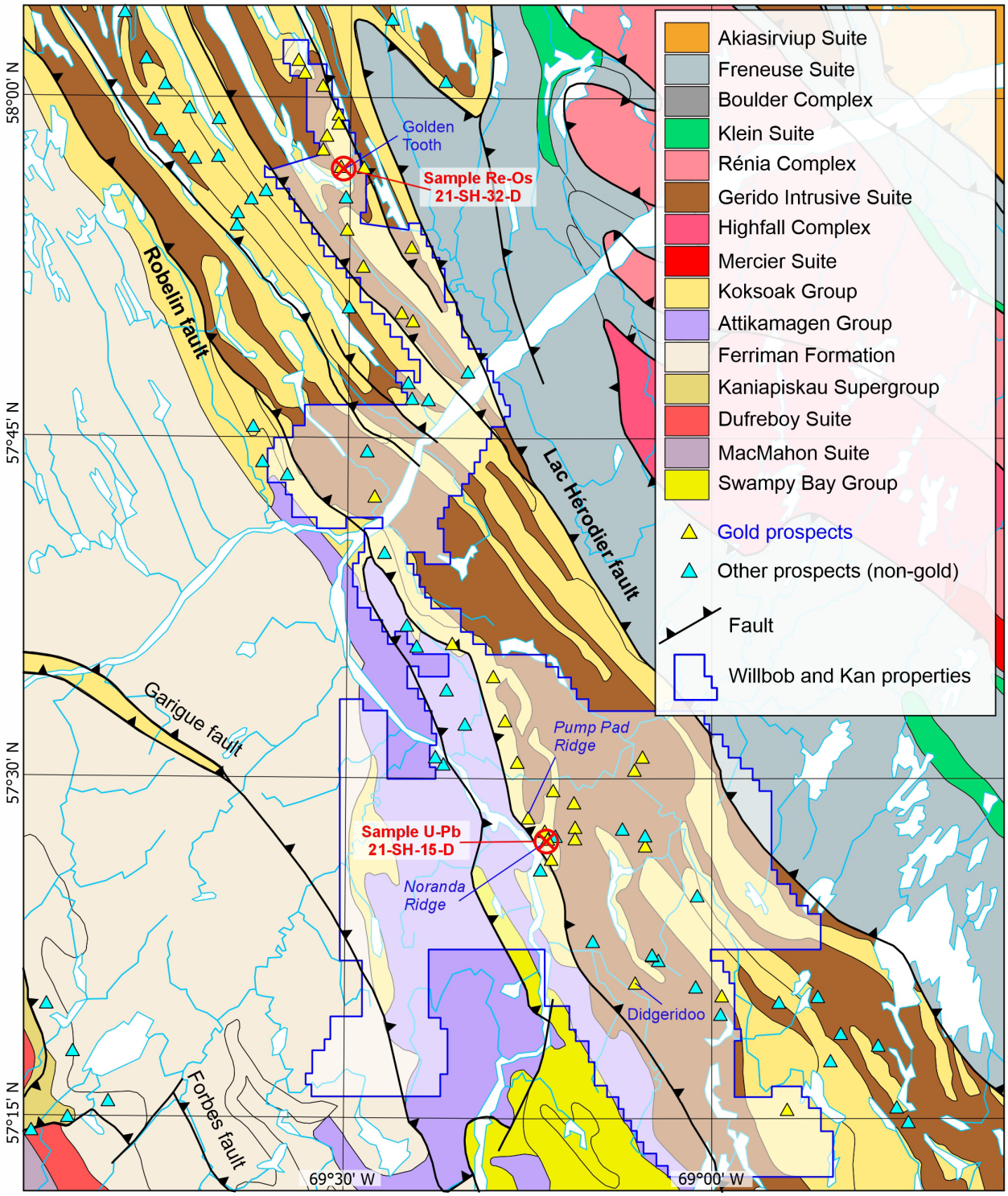

Figure 4. Location of the Kan and Willbob exploration properties, with most gold showings located in the Gérido zone between the lac Hérodier and Robelin early (D_1) thrust faults. Geology and prospects from SIGÉOM (MRNF).

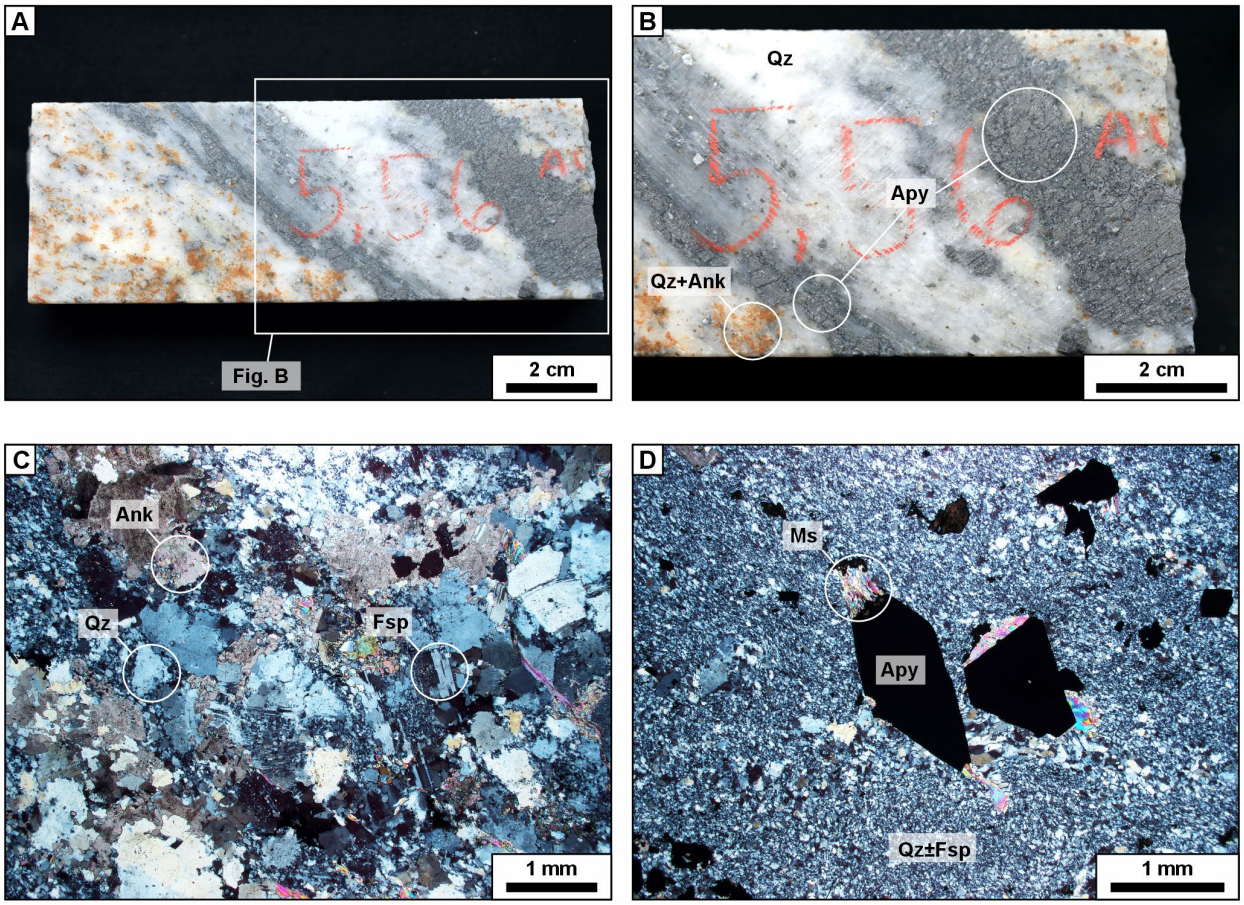

Figure 5. Photographs of sample SH-21-32-D, Golden Tooth prospect, Willbob exploration property. The sample comes from a mineralized interval that consists of quartz-Fe carbonate-feldspar veins containing auriferous arsenopyrite in a variably altered dioritic intrusive body. **A.** Sample SH-21-32-D consisting of a ~10-15 cm-thick quartz, feldspar, and carbonate vein with bands of arsenopyrite crystals. Photograph by P. Mercier-Langevin, NRCan photo 2023-381. **B.** Closer view of the sampled vein and arsenopyrite bands. Photograph by P. Mercier-Langevin, NRCan photo 2023-382. **C.** Photomicrograph (cross-polarized transmitted light) of the mineralized quartz, feldspar, and carbonate vein. Photograph by P. Mercier-Langevin, NRCan photo 2023-383. **D.** Close-up view (photomicrograph, cross-polarized transmitted light) of arsenopyrite crystals with muscovite and quartz-filled pressure shadows indicating the deformation overprinting the arsenopyrite. Photograph by P. Mercier-Langevin, NRCan photo 2023-384. Abbreviations: Ank = ankerite (Fe-carbonate), Apy = arsenopyrite, Au = gold, Fsp = feldspar, Ms = muscovite, Qz = quartz.

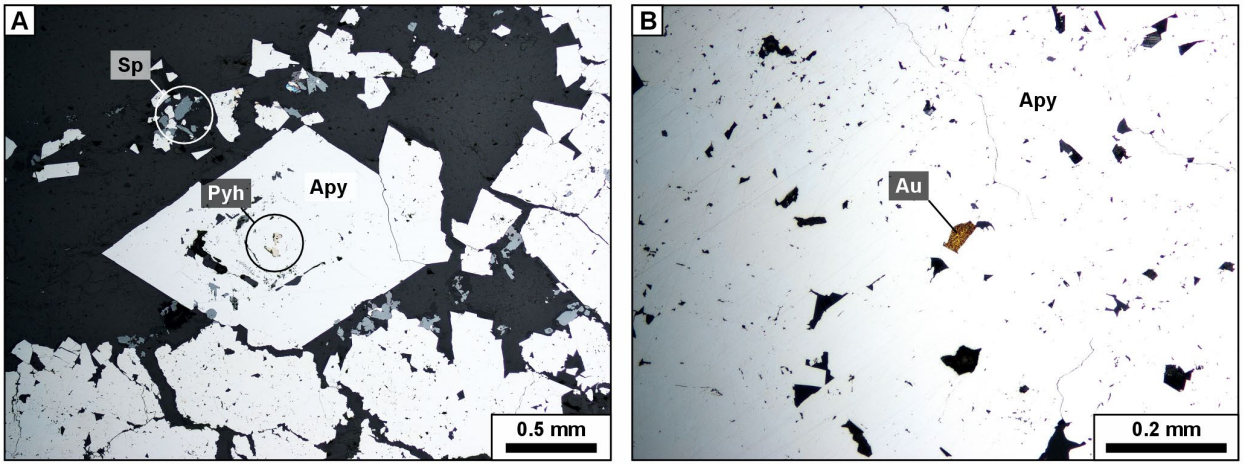

Figure 6. Photographs of sample SH-21-32-D, Golden Tooth prospect, Willbob exploration property. The sample comes from a mineralized interval that consists of quartz-Fe carbonate-feldspar veins containing auriferous arsenopyrite in a variably altered dioritic intrusive body. **A.** Photomicrograph (reflected light) of a complexly zoned arsenopyrite crystal with growth zones, dissolution-reprecipitation (recrystallization) textures, and pyrrhotite inclusions, with traces of sphalerite. Photograph by P. Mercier-Langevin, NRCan photo 2023-385. **B.** Photomicrograph (reflected light) of a recrystallized arsenopyrite crystal with small inclusions of gold (or electrum). Photograph by P. Mercier-Langevin, NRCan photo 2023-386. Abbreviations: Apy = arsenopyrite, Au = gold, Pyh = pyrrhotite, Sp = sphalerite.

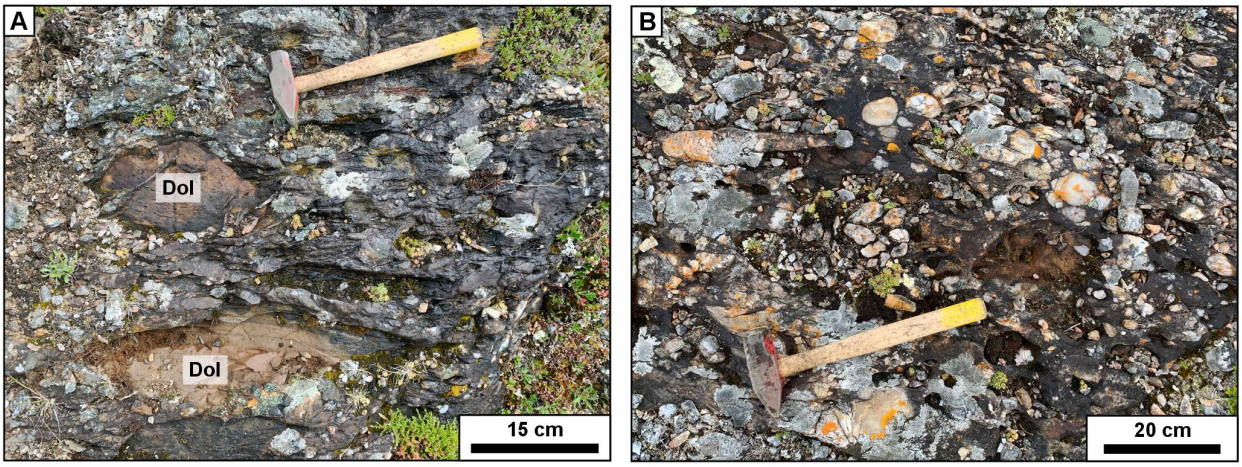

Figure 7. **A.** Field photograph of the Kan conglomerate from which U-Pb geochronology sample SH-21-15-D was collected. The conglomerate is polymictic with large clasts of dolomite (dull brown: Dol) and it is strongly foliated. Photograph by S. Hébert, NRCan photo 2023-387. **B.** Abundant well-rounded chert clasts in the Kan conglomerate. Photograph by S. Hébert, NRCan photo 2023-388.

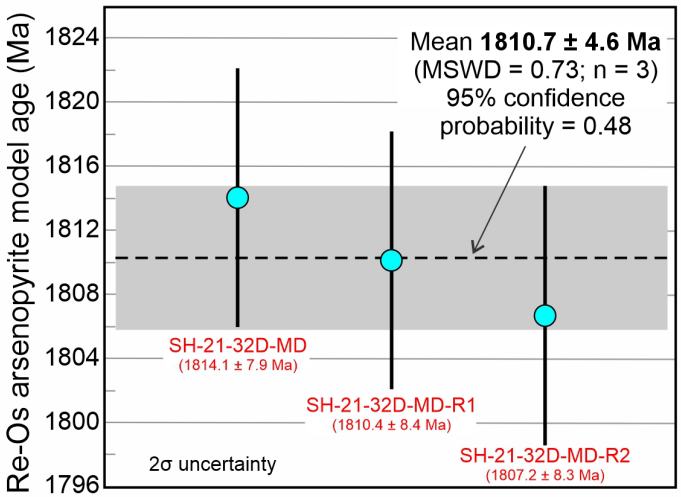

Figure 8. Re-Os arsenopyrite model ages for sample SH-21-32-D. The data yield reproducible Re-Os model ages from 1807 to 1814 Ma that are clearly within analytical uncertainty at 2σ. The three analyses give a weighted average Model Age of 1810.7 ± 4.6 Ma.

Figure 9. A. Concordia diagram showing SHRIMP zircon data age for sample SH-21-15-D, with a photograph of representative zircon grains (inset). **B.** Combined probability density and histogram plot of detrital zircon $^{207}Pb/^{206}Pb$ dates from sample SH-21-15-D showing a strong mode at ca. 2695 Ma and a couple of much smaller ones between ca 2850, 2795, 2640, and 2620 Ma, indicating a dominant Archean source of zircon in the conglomerate. The dark shaded area indicates only data that are within ±5% of confidence. In the instance of replicate analyses of a single crystal, only the weighted mean (or oldest $^{207}Pb/^{206}Pb$ date where a weighted mean could not be calculated) was included in the combined plots. Histogram bin width is 15 Ma.

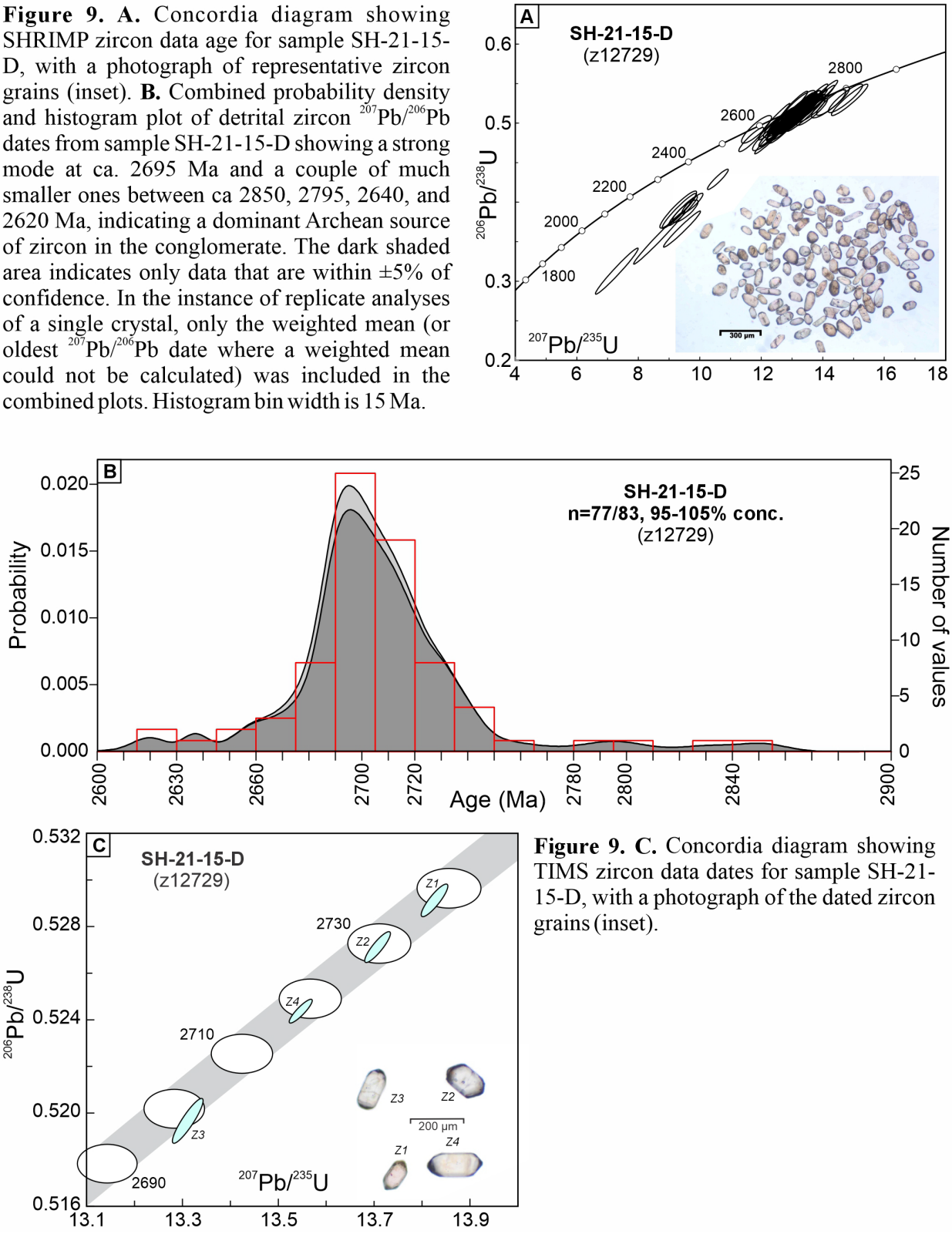

Figure 9. C. Concordia diagram showing TIMS zircon data dates for sample SH-21-15-D, with a photograph of the dated zircon grains (inset).